Biological Psychiatry

Archival Report

Ketamine Rapidly Enhances Glutamate-Evoked Dendritic Spinogenesis in Medial Prefrontal Cortex Through Dopaminergic Mechanisms

Mingzheng Wu, Samuel Minkowicz, Vasin Dumrongprechachan, Pauline Hamilton, and Yevgenia Kozorovitskiy

ABSTRACT

BACKGROUND: Ketamine elicits rapid onset antidepressant effects in patients with clinical depression through mechanisms hypothesized to involve the genesis of neocortical dendritic spines and synapses. Yet, the observed changes in dendritic spine morphology usually emerge well after ketamine clearance, raising questions about the link between rapid behavioral effects of ketamine and plasticity.

METHODS: Here, we used two-photon glutamate uncaging/imaging to focally induce spinogenesis in the medial prefrontal cortex, directly interrogating baseline and ketamine-associated plasticity of deep layer pyramidal neurons in C57BL/6 mice. We combined pharmacological, genetic, optogenetic, and chemogenetic manipulations to interrogate dopaminergic mechanisms underlying ketamine-induced rapid enhancement in evoked plasticity and associated behavioral changes.

RESULTS: We found that ketamine rapidly enhances glutamate-evoked spinogenesis in the medial prefrontal cortex, with timing that matches the onset of its behavioral efficacy and precedes changes in dendritic spine density. Ketamine increases evoked cortical spinogenesis through dopamine Drd1 receptor (Drd1) activation that requires dopamine release, compensating blunted plasticity in a learned helplessness paradigm. The enhancement in evoked spinogenesis after Drd1 activation or ketamine treatment depends on postsynaptic protein kinase A activity. Furthermore, ketamine's behavioral effects are blocked by chemogenetic inhibition of dopamine release and mimicked by activating presynaptic dopaminergic terminals or postsynaptic $G\alpha_s$-coupled cascades in the medial prefrontal cortex.

CONCLUSIONS: Our findings highlight dopaminergic mediation of rapid enhancement in activity-dependent dendritic spinogenesis and behavioral effects induced by ketamine.

https://doi.org/10.1016/j.biopsych.2020.12.022

Ketamine and its S-enantiomer esketamine demonstrate rapid onset and lasting antidepressant effects in clinical studies (1,2); esketamine (Spravato) was recently approved by the U.S. Food and Drug Administration for treatment-resistant depression (3). Ketamine acts primarily as an antagonist at the glutamatergic NMDA receptors (4–8), although several studies implicate mechanisms beyond direct NMDA receptor antagonism (9,10). Ketamine has been shown to ameliorate depressive-like behaviors in animal models of stress (11–15). Accumulating evidence implicates the enhancement of synaptic plasticity in ketamine's behavioral effects (6,8,13,14,16–19). Several prior studies demonstrate that in vivo administration of ketamine enhances dendritic spine density (16,20–23) and restores dendritic spine loss in the medial prefrontal cortex (mPFC) (19). Notably, increased dendritic spine density in mPFC pyramidal neurons usually emerges 12 to 24 hours after a single subanesthetic dose of ketamine (16,19,20,23), yet clinical effects on behavior emerge within 2 to 4 hours (1,2,24). Even if ketamine's effects on plasticity are linked to its behavioral efficacy, as has been suggested (16,19,21,23,25), this temporal mismatch could in principle result from a rapid enhancement of spinogenesis by ketamine, which over time leads to increased dendritic spine density. This possibility has not yet been directly examined.

Changes in hedonic, motivational, and aversive processing represent fundamental features of major depressive disorders (26–29). Reward, aversion, and motivational states are strongly tied to changes in the activity of midbrain dopaminergic neurons (30–35). In addition, dysregulation of dopamine (DA) systems has been demonstrated in patients with clinical depression (36,37) and in animal models of depression (38–41). The reversal of deficits in the DA system usually improves depressive-like behaviors (39,40,42). A recently published meta-analysis suggests that subanesthetic doses of ketamine increase DA levels in the PFC (43), reported for both in vivo and ex vivo studies (44–48). Yet, little is known about the behavioral and neurobiological consequences of elevated cortical dopamine level induced by ketamine treatment. Outside the context of ketamine effects on the brain, several studies have elucidated DA modulation of intrinsic excitability and ion channel

SEE COMMENTARY ON PAGE 1030

 ISSN: 0006-3223

properties of mPFC pyramidal neurons (49–52). Whether DA signaling regulates structural plasticity of dendritic spines in the mPFC and whether changes in DA tone account for ketamine-associated plasticity remain unknown.

Here, we relied on dual laser two-photon glutamate uncaging and imaging to directly induce de novo dendritic spinogenesis on mPFC pyramidal neurons. The spatiotemporal control of this assay enabled us to evaluate the capacity for spinogenesis independently from preexisting dendritic spines. Combining this assay with pharmacological, genetic, and behavioral manipulations allowed us to functionally dissect the underlying mechanism of changes in the glutamate-evoked genesis of new dendritic spines.

METHODS AND MATERIALS

A detailed description of experimental procedures, including mouse strains and genotyping, stereotactic injections and optic fiber implants, behavior assays, local drug infusion, acute slice preparation, pharmacology, tissue processing and immunohistochemistry, and quantitative fluorescence in situ hybridization, is provided in the Supplement.

Mouse Strains and Genotyping

Animals were handled according to protocols approved by the Northwestern University Animal Care and Use Committee. Weanling and young adult male and female mice (postnatal days P25–P60) were used in this study. Approximately equal numbers of male and female mice were used for every experiment. All mice were group housed with standard feeding, light/dark cycle, and enrichment procedures; littermates were randomly assigned to conditions.

Behavior Assays: Learned Helplessness

P40–P60 mice were used for behavioral assays with optogenetic and chemogenetic experiments. P25–P40 mice were used for spinogenesis assays with behavioral manipulations. The learned helplessness (LH) procedure consisted of two induction sessions (one session per day; 360 inescapable foot shocks per session; 0.3 mA, 3 seconds; random 1- to 15-second intershock intervals). Active/Passive Avoidance Shuttle Boxes from Maze Engineers (Boston, MA) were used for the experiment. To assess the degree of aversive learning, test sessions (30 escapable foot shocks per session; 0.3 mA, 10 seconds; random 5- to 30-second intershock intervals) were conducted before induction, 24 hours after the last induction session, and following pharmacological or optogenetic manipulations. The testing was performed in a shuttle box (18 × 18 × 20 cm) equipped with a grid floor and a door separating the two compartments. No conditioned stimulus was delivered either before or after the shocks. Escapes were scored when the animal shuttled between compartments during the shock. Escape latency was measured as the time from the start of the shock to the escape. The shock automatically terminated when the animal shuttled to the other compartment. Failures were scored when the animal failed to escape before the shock end. The weaker LH paradigm (wLH) consisted of one induction session and one test session with a larger number of brief escapable shocks (100 escapable foot shocks per session; 0.3 mA, 3 seconds; random 5- to 15-second intershock intervals). All behavioral assays were conducted during the active phase of the circadian cycle. Schematics involving mice were made using BioRender software (BioRender, Toronto, Ontario, Canada).

Two-Photon Imaging With Two-Photon Glutamate Uncaging

Dendritic imaging and uncaging of MNI-glutamate for spinogenesis induction were accomplished on a custom-built microscope combining two-photon laser-scanning microscopy and two-photon laser photoactivation, as previously described (53–55). Two mode-locked Ti:Sapphire lasers (Mai Tai eHP and Mai Tai eHP DeepSee; Spectra-Physics, Santa Clara, CA) were tuned to 910 and 725 nm for exciting enhanced green fluorescent protein (EGFP) and uncaging MNI-glutamate, respectively. The intensity of each laser was independently controlled by Pockels cells (Conoptics, Danbury, CT). A modified version of ScanImage software was used for data acquisition (56). For glutamate uncaging, 2.5 mM MNI-caged-L-glutamate (Tocris Bioscience, Bristol, UK) was perfused into the slice chamber, and 725 nm light guided through a galvo scanhead was used to focally release the caging group. Secondary and tertiary dendritic branches were selected for dendritic imaging and spinogenesis induction. MNI-glutamate was uncaged near the dendrite (~0.5 μm) at 2 Hz using up to 40 2-ms pulses. Images were continually acquired during the induction protocol at 1 Hz, and uncaging was stopped if a spinehead was visible before 40 uncaging pulses were delivered. Analysis was carried out on raw image stacks and Z projections. For display purposes only, a subset of the two-photon micrographs was processed using Candle (57). A successful induction of new dendritic spine was scored when a protrusion from the dendrite in the uncaging location was observed. A newly generated dendritic spine needed to satisfy the following criteria: de novo protrusion from the dendrite within 1 μm of the uncaging site, mean spine head fluorescence matching average fluorescence of spine heads on the parent dendrite, and mean spine head fluorescence exceeding 20% of intensity in the parent dendrite. Changes in fluorescence intensity were profiled using line-scan analyses. For each animal, the probability of spinogenesis is represented as the fraction of successful induction trials out of all conducted trials within the individual.

Quantification of Dendritic Spine Density

Sections of the mPFC were examined with either a custom-built two-photon laser-scanning microscope or a Leica SP5 confocal microscope (Leica Microsystems). Distal apical dendritic segments were selected for analysis. For each dendritic segment, dendritic spines protruding on both sides of the dendrite were marked using a 3D reconstruction system, Neurolucida 360 (MBF Bioscience, Williston, VT). A total of 6 to 8 Z stacks (0.3 μm between each stack), at 0.07-μm lateral pixel size, were used for reconstruction. Dendritic spine density was averaged from 8 to 12 dendritic segments for each animal.

Statistical Analyses

Group statistical analyses were done using GraphPad Prism 7 software (GraphPad, La Jolla, CA). For *N* sizes, the number of trials and the number of animals are provided. All data are

expressed as mean ± SEM or individual plots. Probabilities are expressed as aggregate probabilities within individuals. For two-group comparisons, statistical significance was determined by two-tailed Student's *t* tests. For multiple group comparisons, one-way or two-way analysis of variance (ANOVA) tests were used for normally distributed data, followed by post hoc analyses. Pearson regression was used to detect the correlation between two groups of data. $p < .05$ was considered statistically significant.

RESULTS

Ketamine Rapidly Enhances Glutamate-Evoked Spinogenesis in mPFC Pyramidal Neurons

Acute slices of the mPFC were prepared from P25–P40 mice of both sexes following neonatal transduction of sparse EGFP expression accomplished by a combination of AAV1.hSyn.Cre and AAV8.FLEX.EGFP. We imaged EGFP-labeled dendrites of layer 5 pyramidal neurons in the mPFC using two-photon laser scanning microscopy (910 nm). A second laser was tuned to 725 nm to locally uncage MNI-glutamate near dendrites to probabilistically induce the formation of new dendritic spines (Figure 1A), as previously described for developing neurons in the striatum and superficial layers of the sensory and motor cortex (53,55,58). Successful and unsuccessful induction trials of de novo spinogenesis were distinguished in Z-stack projections through a dendritic segment before and after the brief induction protocol (<30 seconds) of up to 40 uncaging pulses (Figure 1B). To be classified as newly induced dendritic spines, the new membrane protrusions needed to satisfy several criteria based on location and fluorescence intensity relative to parent dendrite and preexisting dendritic spines (Supplemental Methods and Materials and Figure S1A–C).

We carried out evoked spinogenesis assays in different mice at several time points (2–72 hours) after a single subanesthetic dose of ketamine (10 mg/kg, intraperitoneal [i.p.]). In vivo administration of ketamine in naïve animals enhanced evoked de novo spinogenesis 2 and 4 hours after treatment (Figure 1C), temporally matching the emergence of ketamine's behavioral effects (4,5). This effect was transient; by 12 hours after ketamine was administered, the probability of spinogenesis decreased back to baseline levels. In addition, dendritic spine density was quantified at the same time points. In contrast to the rapid transient changes in evoked spinogenesis, the increase in dendritic spine density was delayed until 12 hours after treatment (Figure 1C), consistent with prior reports (14,18–20). This temporal precedence of ketamine-associated potentiation of evoked spinogenesis suggests that changes in the potential for activity-dependent plasticity may contribute to slower accumulating increases in spine density after ketamine treatment.

Rapid Enhancement in Evoked Spinogenesis Requires Drd1-Protein Kinase A Signaling

Given the hypothesized links between ketamine and the DA system, we sought to determine whether ketamine's effect on evoked plasticity is mediated by the activation of DA receptors. First, we verified the expression of Drd1s in EGFP-expressing neurons. Consistent with prior reports (59,60), the majority of pyramidal neurons in the deep layers of the mPFC express *Drd1a* messenger RNA (mRNA) (Figure 1D and Figure S2A, B). We compared glutamate-evoked spinogenesis after administering ketamine alone or in conjunction with a Drd1 antagonist, SKF 83566 (10 mg/kg i.p., 2 hours prior to ex vivo experiments). We found that antagonizing Drd1s blocked ketamine's potentiation of evoked spinogenesis, while the antagonist treatment alone had no effect relative to baseline (Figure 1D). Thus, while the activation of Drd1s in this neuronal population is not required for baseline glutamate-evoked plasticity, it appears to be necessary for ketamine's enhancement of evoked spinogenesis.

Next, to suppress mPFC DA release without broadly altering Drd1 activation and locomotor behavior (61), we used chemogenetic inhibition of ventral tegmental area (VTA) DA neurons, the major source of DA in the mPFC. Inhibiting hM4Di$^+$ VTA DA neurons with clozapine N-oxide (CNO) (3 mg/kg, i.p.) while administering ketamine treatment blocked ketamine's spinogenesis-enhancing effects (Figure 1E). Yet, as for the pharmacological Drd1 blockade in vivo, we observed no effects of CNO treatment on evoked spinogenesis in the absence of ketamine. These observations are consistent with a model where the genesis of new dendritic spines and synapses mechanistically depends on glutamate, but the enhancement of this plasticity requires the activation of protein kinase A (PKA) via Gα_s-coupled receptors (55). In addition to blocking ketamine-mediated enhancement of evoked spinogenesis, transient inhibition of VTA DA neuron activity (a single CNO dose + ketamine) also abolished the delayed increase of spine density 24 hours after ketamine (Figure 1F). These data show that in the absence of behavioral manipulations, Drd1 activation and VTA DA activity regulate changes in spinogenesis and dendritic spine density, mediating the effects of ketamine on plasticity in the mPFC.

The next series of experiments tested whether the capacity for spinogenesis is altered in animal models of stress, where ketamine ameliorates behavior. We exposed mice to subacute uncontrollable stress by administering foot shocks over 2 days using an adapted model of LH (3 seconds inescapable, 360 shocks each day) (Figure 2A). Following repeated exposure to inescapable foot shocks, LH behavior manifests in increased failures to escape from readily avoidable shocks (10 seconds escapable, 30 trials total), consistent with prior reports (38,62). A single dose of ketamine 4 hours prior to the test (10 mg/kg, i.p.) is sufficient to rescue escape behavior in this paradigm (Figure 2B). We next tested glutamate-evoked spinogenesis in the baseline, after stress exposure (LH), and following ketamine treatment (LH + ketamine). The probability of glutamate-evoked spinogenesis decreased relative to baseline in LH mice, while ketamine treatment restored the baseline potential for plasticity (Figure 2C). We found that 2 days of stressful experience is sufficient to decrease the potential of spinogenesis in mPFC pyramidal neurons, in contrast to changes in dendritic spine density that normally manifest after chronic stress (16,63,64). No significant sex difference was observed across conditions despite a trend toward higher evoked spinogenesis in female mice in the baseline condition (Figure S3A, B). To correlate individual behavioral outcomes with evoked plasticity, we performed de novo spinogenesis

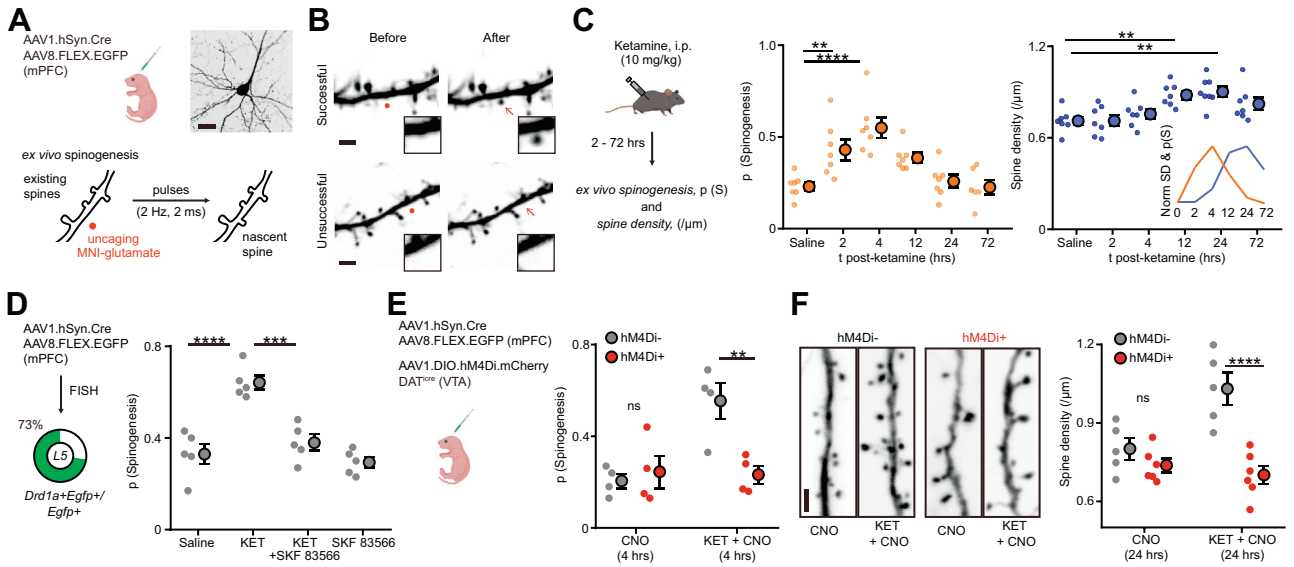

Figure 1. KET regulates mPFC plasticity through a DA-dependent mechanism. **(A)** Schematic illustrating glutamate-evoked de novo spinogenesis platform. Top: viral transduction and an example EGFP$^+$ pyramidal neuron in the mPFC. Bottom: MNI-glutamate uncaging parameters for the induction of new dendritic spines. Scale bar = 50 μm. **(B)** Example two-photon laser-scanning microscopy images of successful and unsuccessful induction trials of de novo spinogenesis. Red circles show uncaging sites. Black rectangles show close-up images of local dendritic segments before and after glutamate uncaging. Scale bar = 2 μm. **(C)** Left: Schematic illustrating time course of KET treatments and experiments. Middle: Time course of evoked spinogenesis probability on deep layer mPFC neurons in mice treated with either saline or KET (10 mg/kg, intraperitoneal, acute slice preparation 2–72 hours after treatment). Each small circle shows aggregate probability of evoked spinogenesis from a single animal. Large circle shows group data. n = 6–7 animals/time point, 15–25 trials/animal, one-way ANOVA, $F_{5,35} = 9.895$, $p < .0001$, Sidak's multiple comparison test vs. saline, 2 hours, $p = .0076$, 4 hours, $p < .0001$, 12 hours, $p = .0532$, 24/72 hours, $p > .90$. Right: Same as left but for dendritic spine density. n = 7–8 animals/time point, one-way ANOVA, $F_{5,37} = 6.319$, $p = .0002$, Sidak's multiple comparison test vs. saline, 2/4 hours, $p > .80$, 12 hours, $p = .0056$, 24 hours, $p = .0011$, 72 hours, $p = .1271$. Inset: Normalized time course of changes in evoked spinogenesis (orange) and dendritic spine density (blue). **(D)** Left: Viral transduction and percentage of *Drd1a*$^+$*Egfp*$^+$/*Egfp*$^+$ cells in layer 5 mPFC. Right: Probability of glutamate-evoked spinogenesis on deep layer mPFC neurons in mice treated with saline, KET (10 mg/kg), KET + SKF 83566 (10 mg/kg), or SKF 83566 alone. Each small circle shows aggregate probability of evoked spinogenesis from a single animal. Large circle shows group data. One-way ANOVA, $p < .0001$, $F_{3,16} = 20.29$, Sidak's multiple comparison test, saline vs. KET, $p < .0001$, KET vs. KET + SKF 83566, $p = .0002$, saline vs. SKF 83566, $p = .8574$. **(E)** Left: Schematic illustrating triple viral transduction strategy for evoked spinogenesis with DA neuron inhibition. Right: Probability of spinogenesis on deep layer mPFC neurons in DAT^{iCre+} and DAT^{iCre-} animals treated with CNO (3 mg/kg) across conditions (baseline and KET). n = 4 animals/condition as shown in plots, two-way ANOVA, Sidak's multiple comparison test, Cre$^-$ vs. Cre$^+$, CNO, $p = .8686$, CNO + KET, $p = .0042$. **(F)** Left: Example confocal images of EGFP expression in dendrites of deep layer mPFC pyramidal neurons in response to CNO and KET treatment, as noted. Scale = 2 μm. Right: same as **(E)** but for dendritic spine density. n = 5–6 animals/condition as shown in plots, two-way ANOVA, Sidak's multiple comparison test, Cre$^-$ vs. Cre$^+$, CNO, $p = .5005$, CNO + KET, $p < .0001$. Scale bar = 2 μm. $^{**}p < .01$, $^{***}p < .001$, $^{****}p < .0001$. Error bars reflect SEM. ANOVA, analysis of variance; CNO, clozapine N-oxide; DA, dopaminergic; EGFP, enhanced green fluorescent protein; FISH, fluorescence in situ hybridization; KET, ketamine; mPFC, medial prefrontal cortex; ns, nonsignificant; t, time; VTA, ventral tegmental area.

assays in animals trained with a modified wLH paradigm with or without subsequent ketamine treatment. In the wLH paradigm, we used a larger number of brief (3-second) escapable foot shocks to evaluate the escape behavior following a single day of LH induction with inescapable shocks (Figure S3C). We found that the probability of evoked spinogenesis negatively correlates with the percentages of failures to escape in both conditions (wLH ± ketamine) (Figure S3D). This result suggests that mPFC plasticity is linked to behavioral profiles of individual animals after LH and ketamine treatment.

We then tested the contribution of Drd1s to ketamine-related plasticity changes. To specifically manipulate Drd1 expression in the mPFC without affecting the global DA system, we conditionally knocked out Drd1s by coexpressing Cre recombinase and Cre-dependent EGFP in Drd1-floxed mice (Figure 2D). We validated the conditional knockout by verifying the expression of *Drd1a* mRNA in EGFP-expressing neurons (Figure 2D). Sparse genetic depletion of Drd1 in mPFC pyramidal neurons abolished ketamine's effect on spinogenesis in LH animals without changing the probability of spinogenesis for mice in the baseline and LH conditions (Figure 2E).

Next, we addressed the downstream signaling mechanism for DA enhancement of glutamate-evoked spinogenesis. Drd1 activation is known to regulate glutamatergic synapse and dendritic spine formation in the developing striatum (55,65). Yet, mPFC Drd1 expression levels in single neurons are considerably lower than in the striatum (mPFC layer 5 pyramidal neurons: ~4/100,000 transcripts; striatum: ~110/100,000) [data from DropViz (66)]. We found that bath application of Drd1 agonist SKF 81297 (1 μM) promotes glutamate-evoked spinogenesis in mPFC pyramidal neurons (Figure 3A, B). This effect requires Drd1 signaling, given that Drd1 conditional knockout abolished the enhancement of spinogenesis. Suppression of PKA activity by either bath application of H-89 (10 μM) or overexpression of endogenous PKA inhibitor (PKIα)

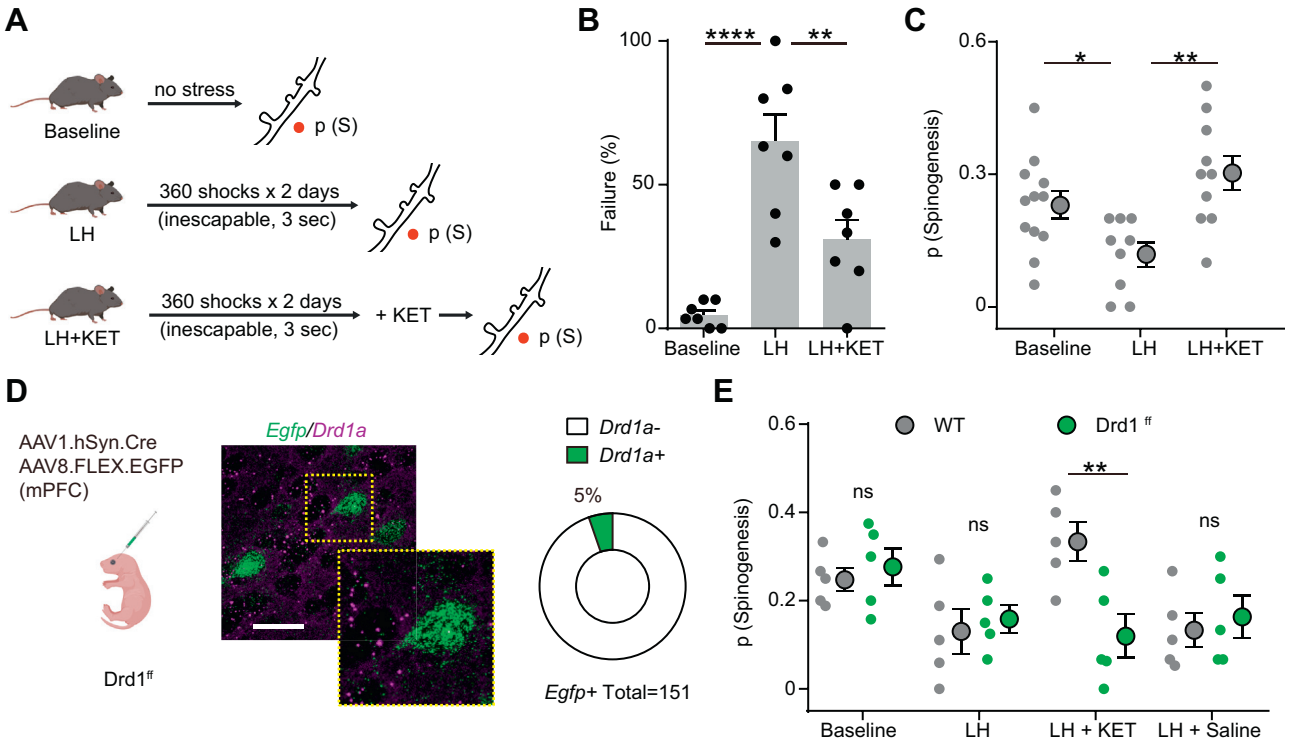

Figure 2. KET rescues mPFC plasticity after stressful experience through dopmanine Drd1 receptor (Drd1). **(A)** Schematic illustrating glutamate-evoked spinogenesis assay in baseline, LH, and LH + KET conditions. **(B)** Summary data showing the percentage of failures to escape an escapable aversive shock, one-way ANOVA, $F_{2,18}$ = 20.26, $p < .0001$, Sidak's multiple comparison test, baseline vs. LH, $p < .0001$, LH vs. LH + KET, $p = .0041$. **(C)** Probability of glutamate-evoked spinogenesis on deep layer mPFC neurons in distinct stages of aversive learning (baseline, LH, and LH + KET). n = 9–12 animals/condition as shown in plots, one-way ANOVA, $F_{2,28} = 7.146$, $p = .0031$, Sidak's multiple comparison test, baseline vs. LH, $p = .0496$, LH vs. LH + KET, $p = .0016$. **(D)** Left: Schematic illustrating dual viral transduction strategy with sparse genetic manipulation of Drd1 expression in Drd1^{ff} mice. Middle: Fluorescence in situ hybridization image confirming the absence of *Drd1a* mRNA expression (purple) in *Egfp* mRNA-expressing mPFC cells (green) in Drd1^{ff} mice. Inset: Close-up of a single neuron. Scale bar = 50 μm. Right: Quantification of the percentage of *Drd1a*$^{+}$ cells among *Egfp*$^{+}$ cells in mPFC. 5% *Drd1a*$^{+}$ and 95% *Drd1a*$^{-}$ among 151 *Egfp*$^{+}$ cells from 2 animals. **(E)** Probability of glutamate-evoked spinogenesis on deep layer mPFC neurons in distinct stages of aversive learning (baseline, LH, LH + KET, and LH + saline) in WT and Drd1^{ff} mice. Two-way ANOVA, Sidak's multiple comparison test, WT vs. Drd1^{ff}, LH + KET, $p = .0043$, baseline, LH and LH + saline, $p > .90$, $n = 5$ animals. *$p < .05$, **$p < .01$, ****$p < .0001$. Error bars reflect SEM. ANOVA, analysis of variance; EGFP, enhanced green fluorescent protein; KET, ketamine; LH, learned helplessness; mPFC, medial prefrontal cortex; mRNA, messenger RNA; ns, nonsignificant; WT, wild-type.

in mPFC pyramidal neurons blocked changes in spinogenesis induced by SKF 81297 (Figure 3B, C). In addition, in vivo pretreatment with ketamine (10 mg/kg, i.p.) occluded the enhancement of spinogenesis by SKF 81297 (Figure 3D), supporting the argument that ketamine's effect on structural plasticity is mediated by Drd1. Furthermore, the plasticity-promoting effect of ketamine was blocked by overexpression of PKIα (Figure 3E). Several established targets of PKA, involved in cytoskeletal remodeling, could contribute to Drd1-dependent effects of ketamine on structural plasticity (67) (Figure 3F). Altogether, our results reveal that ketamine's rapid modulation of structural plasticity in mPFC pyramidal neurons requires the Drd1-PKA signaling cascade.

Bidirectional Manipulation of mPFC DA Release Controls Behavioral Effects of Ketamine

To connect the mechanisms of ketamine-associated plasticity and its behavioral effects, we examined the role of cortical DA signaling in escape behavior after LH. To induce local dopamine release in the mPFC, we optogenetically activated DA terminals in the mPFC in animals with channelrhodopsin-2 expression restricted to VTA DA neurons. DAT^{icre} neonates were transduced with AAV1.EF1α.-DIO.hChR2(H134R).EYFP, or a control fluorophore, and were implanted with optical fibers 4 to 6 weeks after transduction (Figure 4A, B). After LH induction, animals received a series of burst optogenetic stimuli at 20 Hz every 10 seconds (10 pulses, 20-ms pulse width, 500-ms train duration) during the test session consisting of 30 avoidable foot shocks (Figure 4C). The stimulation bursts were not timed relative to shocks and took place on either side of the shuttle box, decreasing the likelihood of forming conditioned place preference or aversion. Optogenetic activation of DA axon terminals in the mPFC significantly decreased the percentage of failures after LH as well as that of latencies to escape (Figure 4D). Optogenetic stimulation did not alter locomotion behavior in either the open field or the shuttle box, suggesting that the high escape tendency is not caused by hyperlocomotion (Figure 4E). Thus, enhancing DA release in the mPFC is sufficient to rescue escapes after LH.

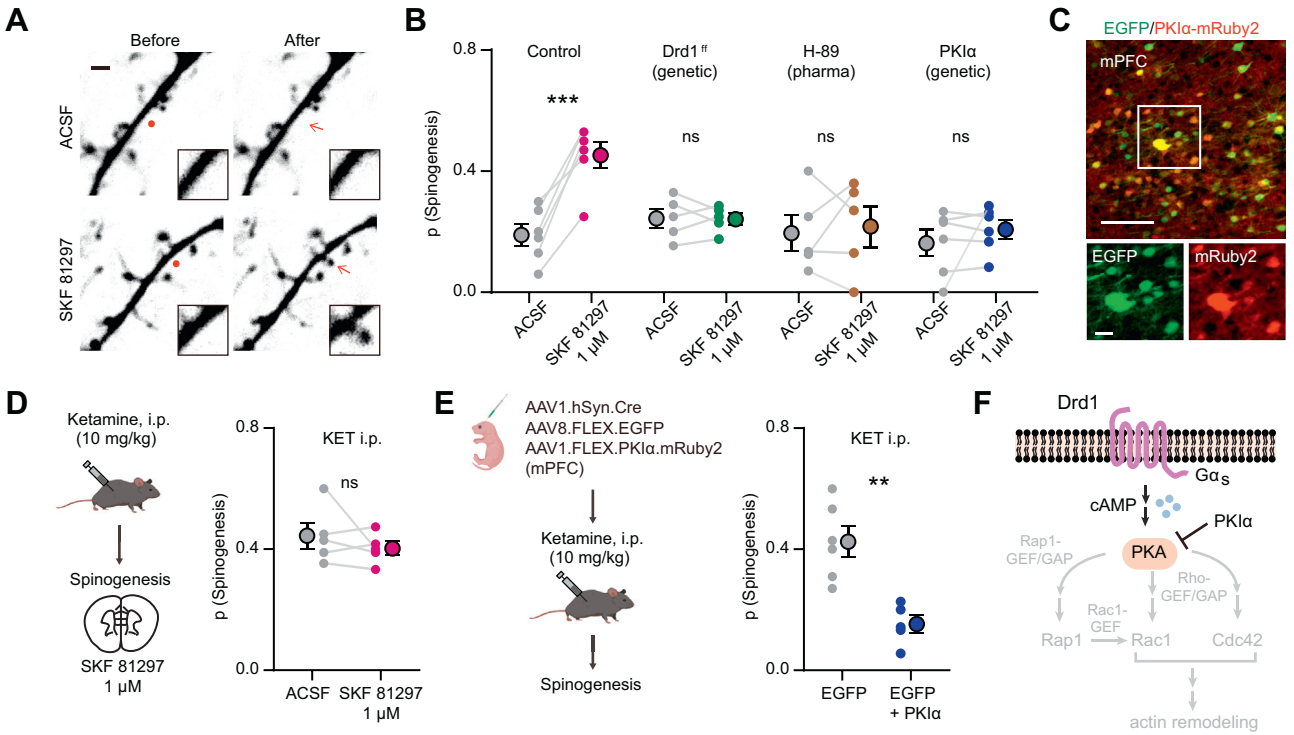

Figure 3. Drd1 activation promotes glutamate-induced spinogenesis in mPFC pyramidal neurons through PKA signaling. **(A)** Example two-photon laser-scanning microscopy images of de novo spinogenesis trials with ACSF or 1 μM SKF 81297. Red circles show uncaging sites. Black rectangle shows close-up images of local dendritic segments before and after glutamate uncaging. Scale bar = 2 μm. **(B)** Probability of glutamate-evoked spinogenesis on deep layer mPFC neurons in brain slices with or without bath application of 1 μM SKF 81297. Slices were treated with 10 μM H-89 or collected from mice with genetic manipulation of GFP-expressing pyramidal neurons (Drd1^{ff} or PKIα). Each small circle shows aggregate probability of evoked spinogenesis from a single experiment. Large circles show group data. Paired two-tailed *t* test, ACSF vs. SKF 81297, control, $p = .0007$, Drd1^{ff}, $p = .9249$, H-89, $p = .7351$, PKIα, $p = .40$; $n = 5$–6 experiments/group. **(C)** Top: Colocalization of PKIα-mRuby2 in EGFP-expressing mPFC neurons. Bottom: Close-up images of EGFP and mRuby2 signals. Scale bars = 100 μm and 20 μm. **(D)** Left: Schematic illustrating glutamate-evoked spinogenesis assay in slices from mice pretreated with KET (10 mg/kg, i.p.). Right: Probability of glutamate-evoked spinogenesis on deep layer mPFC neurons in brain slices with or without bath application of 1 μM SKF 81297. Paired two-tailed *t* test, ACSF vs. SKF 81297, $p = .3745$. **(E)** Left: Schematic illustrating triple viral transduction strategy for PKIα expression. Right: Probability of glutamate-evoked spinogenesis in deep layer mPFC neurons in mice with or without PKIα expression injected with KET (10 mg/kg, i.p.). Unpaired two-tailed *t* test, EGFP vs. EGFP + PKIα, $p = .0020$. **(F)** Schematic of simplified signaling pathways downstream of Drd1-PKA involved in actin remodeling in dendritic spines. $^{**}p < .01$, $^{***}p < .001$. Error bars reflect SEM. ACSF, artificial cerebrospinal fluid; EGFP, enhanced green fluorescent protein; i.p., intraperitoneal; KET, ketamine; mPFC, medial prefrontal cortex; ns, nonsignificant; PKA, protein kinase A; PKIα, α-isoform of PKA inhibitor.

While we found that optogenetically driven increase in mPFC DA tone mimics behavioral effects of ketamine, whether these effects require local DA release in the mPFC remains unclear. To achieve local inhibition of DA release, we infused CNO into the mPFC of mice expressing hM4Di in VTA DA neurons and their terminals in the mPFC to reduce axonal release of dopamine (68–70). DAT^{iCre} neonates were transduced with AAV1.CBA.DIO.hM4Di.mCherry in the VTA, and cannulae were implanted bilaterally over the mPFC in order to locally deliver 1 mM CNO (1 μL for each side) (Figure 4F and Figure S4A). A high density of hM4Di.mCherry expression in mPFC terminals was observed in immunoenhanced fixed tissue sections (Figure 4G). Local infusion of CNO into the mPFC along with ketamine treatment blocked the behavioral effect of ketamine (10 mg/kg, i.p.) in the LH paradigm, while ketamine alone was sufficient to rescue escape behavior (Figure 4H and Figure S4B). To determine whether mPFC DA function is required to maintain the effect of ketamine on behavior, we chemogenetically inhibited DA release 24 hours after ketamine treatment (Figure S4C). This delayed manipulation had no significant effect on escape behaviors. Together, these results suggest that disruption of DA signaling is important for ketamine effects during an initial narrow time window following ketamine administration.

The activation of Drd1s initiates $G\alpha_s$-mediated PKA signaling cascades, which enhance spinogenesis, synaptic transmission, and neuronal activity (54,55,59,71). Therefore, we tested whether selective activation of $G\alpha_s$ signaling in mPFC Drd1-expressing neurons could rescue escape behavior after aversive learning. We relied on the $G\alpha_s$-coupled rM3D DREADD (designer receptor exclusively activated by designer drugs), expressing AAV1.CBA.DIO.rM3Ds.mCherry in Drd1^{Cre} (FK150) mice (Figure 4I). The expression of rM3Ds alone did not change baseline escape and failure rates, nor did the magnitude of aversive learning. After LH induction, a single i.p. dose of CNO (3 mg/kg) was sufficient to rescue escape behavior 4 hours after treatment, lasting at least 24 hours (Figure 4I). Activating $G\alpha_s$ signaling in Drd1-expressing

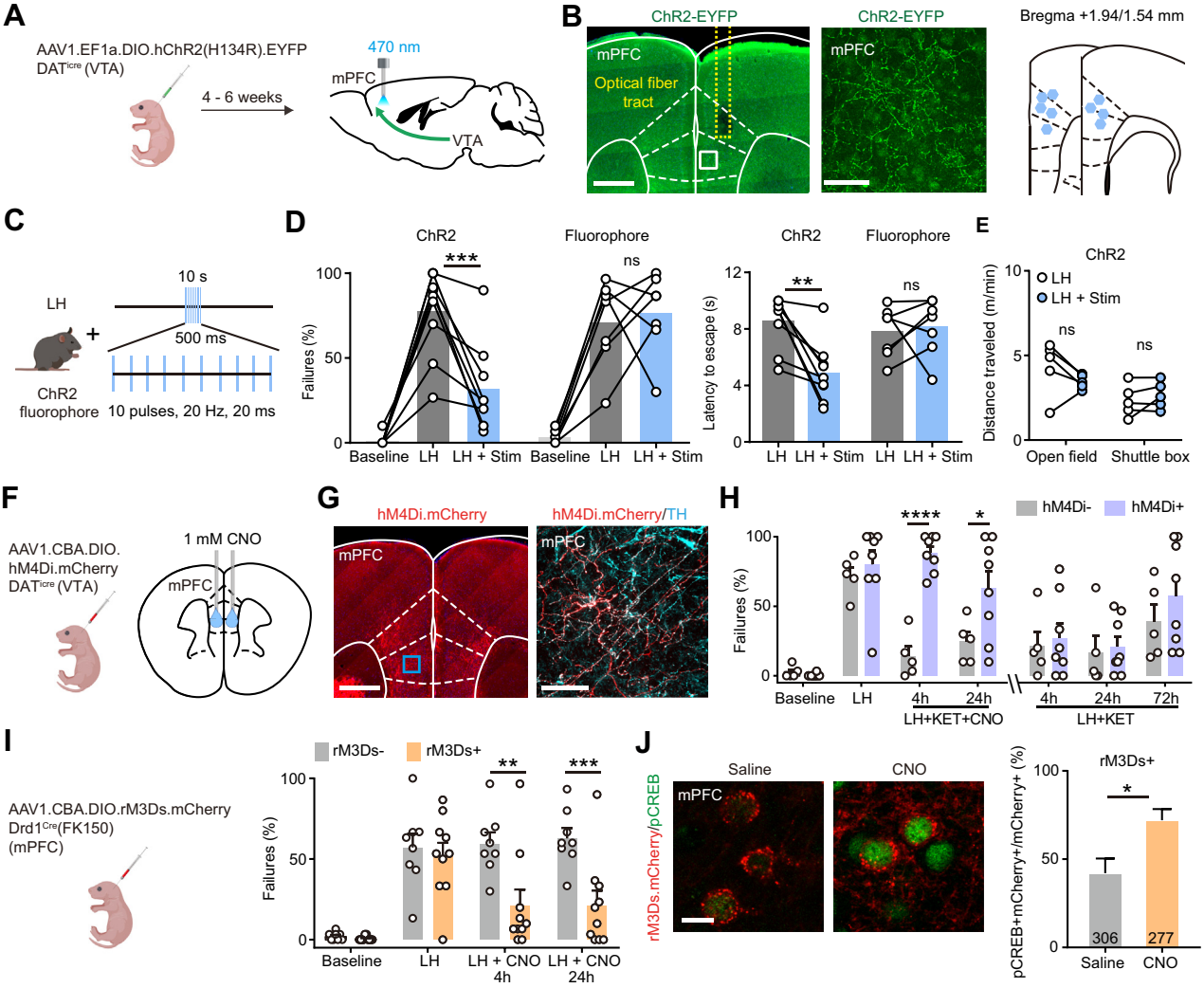

Figure 4. Activity of local dopaminergic terminals and Drd1+ neurons in mPFC mediates KET effects on behavior after stress. **(A)** Schematic for viral transduction with Cre-dependent ChR2 AAV in the VTA and subsequent optogenetic fiber implant in mPFC. **(B)** Left: Fiber placement illustration on a coronal section through mPFC with a close-up image of ChR2.EYFP terminals (white dashed lines: Paxinos atlas overlay; yellow dashed lines: fiber track). Green: immunoenhanced ChR2.EYFP; blue: Hoechst nucleic stain. Scale bars = 500 μm and 50 μm. Right: Atlas location of fiber placement for each subject. **(C)** Schematic illustrating open loop Stim parameters. **(D)** Left: Summary data showing the percentage of failures to escape an escapable aversive shock in ChR2-expressing mice (n = 9) and fluorophore-expressing control mice (n = 7) across phases of learning, baseline, LH, and LH + Stim. Right: Summary data for latency to escape in LH condition compared with LH + Stim condition. Repeated-measures two-way ANOVA, Sidak's multiple comparison test, LH vs. LH + Stim, ChR2, p = .0002, fluorophore, p = .9358. Latency to escape, LH vs. LH + Stim, ChR2, p = .0014, fluorophore, p = .9248. **(E)** Locomotion in the open field and shuttle box (m/min) after learning with and without Stim. Repeated-measures two-way ANOVA, Sidak's multiple comparison test, open field, p = .1742, shuttle box, p = .7503, n = 5 mice. **(F)** Left: Schematic illustrating viral transduction strategy. Right: Local CNO infusion in mPFC (1 mM and 1 μL). **(G)** Left: Immunoenhanced image of hM4Di.mCherry^{+} DAT^{+} terminals in mPFC. Right: mCherry^{+} terminals colocalize with a subset of TH-expressing axons. Scale bars = 500 μm and 50 μm. **(H)** Summary data showing the percentage of failures to escape an escapable aversive shock across learning and treatment conditions for hM4Di-expressing DAT^{iCre} positive and negative littermates. n = 5 animals for Cre^{-} and 8 animals for Cre^{+}, two-way ANOVA, Sidak's multiple comparison test. KET + CNO 4 hours, $p < .0001$, KET + CNO 24 hours, p = .0476, KET only 4, 24, and 72 hours, $p > .70$. **(I)** Left: Schematic illustrating viral transduction strategy. Right: Summary data showing the percentage of failures to escape an escapable aversive shock in Drd1^{Cre+} and Drd1^{Cre-} mice expressing rM3Ds across phases of learning and after CNO treatment (baseline, LH, LH + CNO 4 hours, and LH + CNO 24 hours). n = 8–10 animals/condition, two-way ANOVA, Sidak's multiple comparison test, Cre^{+} vs. Cre^{-}, LH + CNO 4 hours, p = .0018, LH + CNO 24 hours, p = .0007, baseline/LH, $p > .90$. **(J)** Left: Colocalization of pCREB immunolabeling and rM3Ds.mCherry expression in mPFC after saline/CNO treatment in Drd1^{Cre+} mice. Right: Quantification of percentage of pCREB^{+} cells among mCherry^{+} cells. Scale bar = 20 μm. n = 3 animals/condition cell number as noted in each bar, two-tailed unpaired t test, p = .0455. *$p < .05$, **$p < .01$, ***$p < .001$, ****$p < .0001$. Error bars reflect SEM. AAV, adeno-associated virus; ANOVA, analysis of variance; ChR2, channelrhodopsin-2; CNO, clozapine N-oxide; EYFP, enhanced yellow fluorescent protein; KET, ketamine; LH, learned helplessness; mPFC, medial prefrontal cortex; ns, nonsignificant; Stim, optogenetic stimulation; TH, tyrosine hydroxylase; VTA, ventral tegmental area.

neurons in vivo significantly increased phosphorylation of CREB (cAMP-response element binding protein), which is typically induced by $G\alpha_s$-coupled cascades (Figure 4J). In addition to our results, a recently published study showed that optogenetic activation of $Drd1^+$ mPFC neurons decreases immobility time in the forced swim test, suggesting that these Drd1-expressing neurons may broadly regulate aversive or active coping responses (72). Altogether, our data demonstrate that mPFC DA signaling mediates both the rapid plasticity-promoting actions and behavioral effects of ketamine.

DISCUSSION

Glutamate-evoked interrogation of plasticity on genetically targeted neurons offers unique strengths as a structural plasticity readout. Besides dissociating de novo genesis and elimination of dendritic spines and synapses, this assay facilitates pharmacological and genetic mechanism dissection and is compatible with behavioral manipulations. Our observations demonstrate a temporal precedence of spinogenesis increase relative to changes in dendritic spine density, suggesting that the changes in spine density in vivo can be due to a prior accumulating change in glutamatergic activity-dependent spinogenesis. Recent work demonstrates that newly formed dendritic spines are required to maintain the behavioral effect of ketamine after chronic corticosterone administration (19), establishing a causal link between the increase in new spine formation and ketamine's behavioral effects. Here, we have defined the mechanisms underlying rapid changes in spinogenesis that are required for these causal effects.

The current study explains several intriguing temporal observations about ketamine actions and reconciles previously reported temporal mismatches. First, rapid antidepressant effects of ketamine usually begin 2 to 4 hours after a single dose of treatment (2,4,24,73), while changes in dendritic spine morphology in the mPFC are primarily observed 8 to 16 hours later (14,16,19,23). Our results reveal that the enhancement of glutamate-induced spinogenesis occurs rapidly (2–4 hours) after ketamine treatment, corresponding to its rapid-onset behavioral effects. Second, the half-life of ketamine is estimated at 1 to 3 hours in humans (~1.5 hours in rodents), with a relatively short clearance time (~8–12 hours) (74,75). These short clearance times stand in contrast to the lasting behavioral effects of ketamine in both humans and rodents (>24 hours) (1,2,24). Given this temporal difference, one intriguing possibility is that the timing of the clinical antidepressant effects of ketamine in patients with major depressive disorder (~1 week following a single dose) derives from a lasting change in DA-dependent structural plasticity caused by ketamine. Exactly how new dendritic spines stabilize and contribute to behavior after ketamine treatment may further reveal how ketamine's effects last days beyond its bioavailability. Because our experiments were carried out in young animals and neural plasticity dynamics are known to change across age (76–78), the efficacy of ketamine treatment could vary in clinical populations as a function of age even if mechanisms of action are conserved. Because DA tone in the mPFC changes through the life span (79–82), the variance in ketamine's antidepressant efficacy [e.g., low efficacy and more transient effects for geriatric depression (83)] may be partially explained by the age-related alterations in cortical DA tone.

This work ties into a growing body of literature explicitly and implicitly linking ketamine, behavior, and plasticity. A recent study concluded that Drd1-positive neurons in the mPFC regulate depressive-like behavior (72), and our study investigated the underlying neuromodulatory and plasticity mechanisms consistent with this discovery. Together, the two studies support the idea that ketamine controls mPFC plasticity and behaviors through cortical modulation by DA. Another recent study demonstrated that newly formed dendritic spines are required to maintain the behavioral effect of ketamine after chronic corticosterone administration (19), establishing a causal link between the increase in new spine formation and ketamine's behavioral effects. These findings, together with our observations of correlated spinogenesis and escape behavior after LH, highlight the importance of new dendritic spine formation for behavioral regulation. Future experiments are required to fully understand the impact of individual variability in plasticity and neuromodulatory signaling on the antidepressant effects of ketamine.

Our observation that DA signaling mediates dendritic spine plasticity in the mPFC after ketamine injection may reflect broadly conserved mechanisms in the brain, where DA controls activity-induced plasticity of dendritic spines and excitatory synapse formation. Prior data demonstrate that during development, DA regulates the formation of dendritic spines and excitatory synapses in striatal direct pathway spiny projection neurons expressing Drd1s (55,65). The activation of Drd1s stimulates $G\alpha_s$ signaling cascades, increasing cAMP production and PKA activity. Analogously, DA promotes glutamate-evoked spinogenesis on mPFC pyramidal neurons through Drd1 activation and changes in PKA activity. Given that actin dynamics are important for dendritic spine formation and shape regulation (84), the mechanistic link between Drd1-PKA signaling and dendritic spine formation likely involves cytoskeleton remodeling proteins. Indeed, PKA modulates the activity of small GTPases (e.g., Rap1, Rac1, Cdc42) known to regulate dendritic spines (67) through guanine nucleotide exchange factors and GTPase-activating proteins (85,86). Specific molecular effectors responsible for ketamine-induced changes in synaptic and dendritic spine plasticity remain to be elucidated and may provide new clinical targets.

ACKNOWLEDGMENTS AND DISCLOSURES

This work was supported by the Rita Allen Foundation Scholar Award (Grant No. NINDS R01NS107539), Searle Scholar Award, Beckman Young Investigator Award, William and Bernice E. Bumpus Young Innovator Award, NARSAD Young Investigator Grant, and P&S Fund Grant (all to YK). MW was supported as an affiliate fellow of the National Institutes of Health (Grant No. T32 AG20506), SM is a fellow of the National Science Foundation Graduate Research Fellowship (Grant No. DGE-1842165), and VD is a predoctoral fellow of the American Heart Association (Grant No. 19PRE34380056).

We are grateful to Lindsey Butler for mouse colony management and to the Northwestern Biological Imaging Facility and Tiffany Schmidt for confocal microscope access.

The authors report no biomedical financial interests or potential conflicts of interest.

A part of this study, along with additional data, was published as a preprint on bioRxiv: https://www.biorxiv.org/content/10.1101/2020.03.11.987818v2.full.

ARTICLE INFORMATION

From the Department of Neurobiology, Northwestern University, Evanston, Illinois.

Address correspondence to Yevgenia Kozorovitskiy, Ph.D., at Yevgenia.Kozorovitskiy@northwestern.edu.

Received Oct 12, 2020; revised Dec 14, 2020; accepted Dec 28, 2020.

Supplementary material cited in this article is available online at https://doi.org/10.1016/j.biopsych.2020.12.022.

REFERENCES

1. Daly EJ, Singh JB, Fedgchin M, Cooper K, Lim P, Shelton RC, *et al.* (2018): Efficacy and safety of intranasal esketamine adjunctive to oral antidepressant therapy in treatment-resistant depression: A randomized clinical trial. JAMA Psychiatry 75:139–148.
2. Berman RM, Cappiello A, Anand A, Oren DA, Heninger GR, Charney DS, Krystal JH (2000): Antidepressant effects of ketamine in depressed patients. Biol Psychiatry 47:351–354.
3. Kim J, Farchione T, Potter A, Chen Q, Temple R (2019): Esketamine for treatment-resistant depression—First FDA-approved antidepressant in a new class. N Engl J Med 381:1–4.
4. Duman RS (2018): Ketamine and rapid-acting antidepressants: A new era in the battle against depression and suicide. F1000Research 7:659.
5. Zanos P, Gould TD (2018): Mechanisms of ketamine action as an antidepressant. Mol Psychiatry 23:801–811.
6. Miller OH, Yang L, Wang C-C, Hargroder EA, Zhang Y, Delpire E, Hall BJ (2014): GluN2B-containing NMDA receptors regulate depression-like behavior and are critical for the rapid antidepressant actions of ketamine. eLife 3:e3581.
7. Abdallah CG, Sanacora G, Duman RS, Krystal JH (2015): Ketamine and rapid-acting antidepressants: A window into a new neurobiology for mood disorder therapeutics. Annu Rev Med 66:509–523.
8. Holmes SE, Scheinost D, Finnema SJ, Naganawa M, Davis MT, DellaGioia N, *et al.* (2019): Lower synaptic density is associated with depression severity and network alterations. Nat Commun 10:1529.
9. Zanos P, Moaddel R, Morris PJ, Georgiou P, Fischell J, Elmer GI, *et al.* (2016): NMDAR inhibition-independent antidepressant actions of ketamine metabolites. Nature 533:481–486.
10. Wray NH, Schappi JM, Singh H, Senese NB, Rasenick MM (2019): NMDAR-independent, cAMP-dependent antidepressant actions of ketamine. Mol Psychiatry 24:1833–1843.
11. Harmer CJ, Duman RS, Cowen PJ (2017): How do antidepressants work? New perspectives for refining future treatment approaches. Lancet Psychiatry 4:409–418.
12. Fuchikami M, Thomas A, Liu R, Wohleb ES, Land BB, DiLeone RJ, *et al.* (2015): Optogenetic stimulation of infralimbic PFC reproduces ketamine's rapid and sustained antidepressant actions. Proc Natl Acad Sci U S A 112:8106–8111.
13. Duman RS, Aghajanian GK (2012): Synaptic dysfunction in depression: Potential therapeutic targets. Science 338:68–72.
14. Duman RS, Aghajanian GK, Sanacora G, Krystal JH (2016): Synaptic plasticity and depression: New insights from stress and rapid-acting antidepressants. Nat Med 22:238–249.
15. Krishnan V, Nestler EJ (2011): Animal models of depression: Molecular perspectives. Curr Top Behav Neurosci 7:121–147.
16. Li N, Lee B, Liu R-J, Banasr M, Dwyer JM, Iwata M, *et al.* (2010): mTOR-dependent synapse formation underlies the rapid antidepressant effects of NMDA antagonists. Science 329:959–964.
17. Popoli M, Yan Z, McEwen BS, Sanacora G (2012): The stressed synapse: The impact of stress and glucocorticoids on glutamate transmission. Nat Rev Neurosci 13:22–37.
18. Gerhard DM, Wohleb ES, Duman RS (2016): Emerging treatment mechanisms for depression: Focus on glutamate and synaptic plasticity. Drug Discov Today 21:454–464.
19. Moda-Sava RN, Murdock MH, Parekh PK, Fetcho RN, Huang BS, Huynh TN, *et al.* (2019): Sustained rescue of prefrontal circuit dysfunction by antidepressant-induced spine formation. Science 364:eaat8078.
20. Phoumthipphavong V, Barthas F, Hassett S, Kwan AC (2016): Longitudinal effects of ketamine on dendritic architecture in vivo in the mouse medial frontal cortex. eNeuro 3:91–95.
21. Sarkar A, Kabbaj M (2016): Sex differences in effects of ketamine on behavior, spine density, and synaptic proteins in socially isolated rats. Biol Psychiatry 80:448–456.
22. Ng LHL, Huang Y, Han L, Chang RC-C, Chan YS, Lai CSW (2018): Ketamine and selective activation of parvalbumin interneurons inhibit stress-induced dendritic spine elimination. Transl Psychiatry 8:272.
23. Liu RJ, Fuchikami M, Dwyer JM, Lepack AE, Duman RS, Aghajanian GK (2013): GSK-3 inhibition potentiates the synaptogenic and antidepressant-like effects of subthreshold doses of ketamine. Neuropsychopharmacology 38:2268–2277.
24. Krystal JH, Sanacora G, Duman RS (2013): Rapid-acting glutamatergic antidepressants: The path to ketamine and beyond. Biol Psychiatry 73:1133–1141.
25. Krystal JH, Abdallah CG, Sanacora G, Charney DS, Duman RS (2019): Ketamine: A paradigm shift for depression research and treatment. Neuron 101:774–778.
26. Proulx CD, Hikosaka O, Malinow R (2014): Reward processing by the lateral habenula in normal and depressive behaviors. Nat Neurosci 17:1146–1152.
27. Abler B, Erk S, Herwig U, Walter H (2007): Anticipation of aversive stimuli activates extended amygdala in unipolar depression. J Psychiatr Res 41:511–522.
28. Heldt SA, Stanek L, Chhatwal JP, Ressler KJ (2007): Hippocampus-specific deletion of BDNF in adult mice impairs spatial memory and extinction of aversive memories. Mol Psychiatry 12:656–670.
29. Luking KR, Pagliaccio D, Luby JL, Barch DM (2016): Reward processing and risk for depression across development. Trends Cogn Sci 20:456–468.
30. Morales M, Margolis EB (2017): Ventral tegmental area: Cellular heterogeneity, connectivity and behaviour. Nat Rev Neurosci 18:73–85.
31. Berridge KC, Kringelbach ML (2015): Pleasure systems in the brain. Neuron 86:646–664.
32. Bromberg-Martin ES, Matsumoto M, Hikosaka O (2010): Dopamine in motivational control: Rewarding, aversive, and alerting. Neuron 68:815–834.
33. de Jong JW, Afjei SA, Pollak Dorocic I, Peck JR, Liu C, Kim CK, *et al.* (2019): A neural circuit mechanism for encoding aversive stimuli in the mesolimbic dopamine system. Neuron 101:133–151.e7.
34. Lammel S, Lim BK, Malenka RC (2014): Reward and aversion in a heterogeneous midbrain dopamine system. Neuropharmacology 76:351–359.
35. Vander Weele CM, Siciliano CA, Matthews GA, Namburi P, Izadmehr EM, Espinel IC, *et al.* (2018): Dopamine enhances signal-to-noise ratio in cortical-brainstem encoding of aversive stimuli. Nature 563:397–401.
36. Dunlop BW, Nemeroff CB (2007): The role of dopamine in the pathophysiology of depression. Arch Gen Psychiatry 64:327–337.
37. Dailly E, Chenu F, Renard CE, Bourin M (2004): Dopamine, depression and antidepressants. Fundam Clin Pharmacol 18:601–607.
38. Belujon P, Grace AA (2014): Restoring mood balance in depression: Ketamine reverses deficit in dopamine-dependent synaptic plasticity. Biol Psychiatry 76:927–936.
39. Chaudhury D, Walsh JJ, Friedman AK, Juarez B, Ku SM, Koo JW, *et al.* (2013): Rapid regulation of depression-related behaviours by control of midbrain dopamine neurons. Nature 493:532–536.
40. Tye KM, Mirzabekov JJ, Warden MR, Ferenczi EA, Tsai H-C, Finkelstein J, *et al.* (2012): Dopamine neurons modulate neural encoding and expression of depression-related behaviour. Nature 493:537–541.
41. Belujon P, Grace AA (2017): Dopamine system dysregulation in major depressive disorders. Int J Neuropsychopharmacol 20:1036–1046.
42. Friedman AK, Walsh JJ, Juarez B, Ku SM, Chaudhury D, Wang J, *et al.* (2014): Enhancing depression mechanisms in midbrain dopamine neurons achieves homeostatic resilience. Science 344:313–319.
43. Kokkinou M, Ashok AH, Howes OD (2018): The effects of ketamine on dopaminergic function: Meta-analysis and review of the implications for neuropsychiatric disorders. Mol Psychiatry 23:59–69.

44. Moghaddam B, Adams B, Verma A, Daly D (1997): Activation of glutamatergic neurotransmission by ketamine: A novel step in the pathway from NMDA receptor blockade to dopaminergic and cognitive disruptions associated with the prefrontal cortex. J Neurosci 17:2921–2927.
45. Verma A, Moghaddam B (1996): NMDA receptor antagonists impair prefrontal cortex function as assessed via spatial delayed alternation performance in rats: Modulation by dopamine. J Neurosci 16:373–379.
46. Chatterjee M, Verma R, Ganguly S, Palit G (2012): Neurochemical and molecular characterization of ketamine-induced experimental psychosis model in mice. Neuropharmacology 63:1161–1171.
47. Lindefors N, Barati S, O'Connor WT (1997): Differential effects of single and repeated ketamine administration on dopamine, serotonin and GABA transmission in rat medial prefrontal cortex. Brain Res 759:205–212.
48. Lorrain D, Baccei C, Bristow L, Anderson J, Varney M (2003): Effects of ketamine and N-methyl-D-aspartate on glutamate and dopamine release in the rat prefrontal cortex: Modulation by a group II selective metabotropic glutamate receptor agonist LY379268. Neuroscience 117:697–706.
49. Tseng KY, O'Donnell P (2004): Dopamine-glutamate interactions controlling prefrontal cortical pyramidal cell excitability involve multiple signaling mechanisms. J Neurosci 24:5131–5139.
50. Wang J, O'Donnell P (2001): D1 dopamine receptors potentiate NMDA-mediated excitability increase in layer V prefrontal cortical pyramidal neurons. Cereb Cortex 11:452–462.
51. Gulledge AT, Jaffe DB (2001): Multiple effects of dopamine on layer V pyramidal cell excitability in rat prefrontal cortex. J Neurophysiol 86:586–595.
52. Chen L, Bohanick JD, Nishihara M, Seamans JK, Yang CR (2007): Dopamine D1/5 receptor-mediated long-term potentiation of intrinsic excitability in rat prefrontal cortical neurons: Ca^{2+}-dependent intracellular signaling. J Neurophysiol 97:2448–2464.
53. Kwon H-B, Sabatini BL (2011): Glutamate induces de novo growth of functional spines in developing cortex. Nature 474:100–104.
54. Kozorovitskiy Y, Saunders A, Johnson CA, Lowell BB, Sabatini BL (2012): Recurrent network activity drives striatal synaptogenesis. Nature 485:646–650.
55. Kozorovitskiy Y, Peixoto R, Wang W, Saunders A, Sabatini BL (2015): Neuromodulation of excitatory synaptogenesis in striatal development. eLife 4:e10111.
56. Pologruto TA, Sabatini BL, Svoboda K (2003): ScanImage: Flexible software for operating laser scanning microscopes. Biomed Eng Online 2:13.
57. Coupé P, Munz M, Manjón JV, Ruthazer ES, Collins DL (2012): A CANDLE for a deeper in vivo insight. Med Image Anal 16:849–864.
58. Guo L, Xiong H, Kim J-I, Wu Y-W, Lalchandani RR, Cui Y, *et al.* (2015): Dynamic rewiring of neural circuits in the motor cortex in mouse models of Parkinson's disease. Nat Neurosci 18:1299–1309.
59. Tritsch NX, Sabatini BL (2012): Dopaminergic modulation of synaptic transmission in cortex and striatum. Neuron 76:33–50.
60. Santana N, Mengod G, Artigas F (2009): Quantitative analysis of the expression of dopamine D1 and D2 receptors in pyramidal and GABAergic neurons of the rat prefrontal cortex. Cereb Cortex 19:849–860.
61. Waddington JL (1986): Behavioural correlates of the action of selective D-1 dopamine receptor antagonists: Impact of SCH 23390 and SKF 83566, and functionally interactive D-1:D-2 receptor systems. Biochem Pharmacol 35:3661–3667.
62. Chourbaji S, Zacher C, Sanchis-Segura C, Dormann C, Vollmayr B, Gass P (2005): Learned helplessness: Validity and reliability of depressive-like states in mice. Brain Res Protoc 16:70–78.
63. Radley JJ, Rocher AB, Miller M, Janssen WGM, Liston C, Hof PR, *et al.* (2006): Repeated stress induces dendritic spine loss in the rat medial prefrontal cortex. Cereb Cortex 16:313–320.
64. Radley JJ, Rocher AB, Rodriguez A, Ehlenberger DB, Dammann M, McEwen BS, *et al.* (2008): Repeated stress alters dendritic spine morphology in the rat medial prefrontal cortex. J Comp Neurol 507:1141–1150.
65. Fasano C, Bourque MJ, Lapointe G, Leo D, Thibault D, Haber M, *et al.* (2013): Dopamine facilitates dendritic spine formation by cultured striatal medium spiny neurons through both D1 and D2 dopamine receptors. Neuropharmacology 67:432–443.
66. Saunders A, Macosko EZ, Wysoker A, Goldman M, Krienen FM, de Rivera H, *et al.* (2018): Molecular diversity and specializations among the cells of the adult mouse brain. Cell 174:1015–1030.e16.
67. Woolfrey KM, Srivastava DP (2016): Control of dendritic spine morphological and functional plasticity by small GTPases. Neural Plast 2016:3025948.
68. Stachniak TJ, Ghosh A, Sternson SM (2014): Chemogenetic synaptic silencing of neural circuits localizes a hypothalamus→midbrain pathway for feeding behavior. Neuron 82:797–808.
69. Mahler SV, Vazey EM, Beckley JT, Keistler CR, McGlinchey EM, Kaufling J, *et al.* (2014): Designer receptors show role for ventral pallidum input to ventral tegmental area in cocaine seeking. Nat Neurosci 17:577–585.
70. Roth BL (2016): DREADDs for neuroscientists. Neuron 89:683–694.
71. Shen W, Flajolet M, Greengard P, Surmeier DJ (2008): Dichotomous dopaminergic control of striatal synaptic plasticity. Science 321:848–851.
72. Hare BD, Shinohara R, Liu RJ, Pothula S, DiLeone RJ, Duman RS (2019): Optogenetic stimulation of medial prefrontal cortex Drd1 neurons produces rapid and long-lasting antidepressant effects. Nat Commun 10:223.
73. Feder A, Parides MK, Murrough JW, Perez AM, Morgan JE, Saxena S, *et al.* (2014): Efficacy of intravenous ketamine for treatment of chronic posttraumatic stress disorder. JAMA Psychiatry 71:681–688.
74. Peltoniemi MA, Hagelberg NM, Olkkola KT, Saari TI (2016): Ketamine: A review of clinical pharmacokinetics and pharmacodynamics in anesthesia and pain therapy. Clin Pharmacokinet 55:1059–1077.
75. Veilleux-Lemieux D, Castel A, Carrier D, Beaudry F, Vachon P (2013): Pharmacokinetics of ketamine and xylazine in young and old Sprague-Dawley rats. J Am Assoc Lab Anim Sci 52:567–570.
76. Wahlstrom D, Collins P, White T, Luciana M (2010): Developmental changes in dopamine neurotransmission in adolescence: Behavioral implications and issues in assessment. Brain Cogn 72:146–159.
77. Freitas C, Perez J, Knobel M, Tormos JM, Oberman L, Eldaief M, *et al.* (2011): Changes in cortical plasticity across the lifespan. Front Aging Neurosci 3:1–8.
78. Li SC, Lindenberger U, Bäckman L (2010): Dopaminergic modulation of cognition across the life span. Neurosci Biobehav Rev 34:625–630.
79. Spear LP (2000): The adolescent brain and age-related behavioral manifestations. Neurosci Biobehav Rev 24:417–463.
80. Kalsbeek A, Voorn P, Buijs RM, Pool CW, Uylings HBM (1988): Development of the dopaminergic innervation in the prefrontal cortex of the rat. J Comp Neurol 269:58–72.
81. MacDonald SWS, Karlsson S, Rieckmann A, Nyberg L, Backman L (2012): Aging-related increases in behavioral variability: Relations to losses of dopamine D1 receptors. J Neurosci 32:8186–8191.
82. Rothmond DA, Weickert CS, Webster MJ (2012): Developmental changes in human dopamine neurotransmission: Cortical receptors and terminators. BMC Neurosci 13:18.
83. Bryant KA, Altinay M, Finnegan N, Cromer K, Dale RM (2019): Effects of repeated intravenous ketamine in treatment-resistant geriatric depression. J Clin Psychopharmacol 39:158–161.
84. Konietzny A, Bär J, Mikhaylova M (2017): Dendritic actin cytoskeleton: Structure, functions, and regulations. Front Cell Neurosci 11:147.
85. Bachmann VA, Riml A, Huber RG, Baillie GS, Liedl KR, Valovka T, Stefan E (2013): Reciprocal regulation of PKA and Rac signaling. Proc Natl Acad Sci U S A 110:8531–8536.
86. Nagai T, Nakamuta S, Kuroda K, Nakauchi S, Nishioka T, Takano T, *et al.* (2016): Phosphoproteomics of the dopamine pathway enables discovery of Rap1 activation as a reward signal in vivo. Neuron 89:550–565.